Supporting Information

Rh/ZrP_2O_7 as an Efficient Automotive Catalyst for NO_x Reduction under Slightly Lean Conditions

Yuki Nagao,[†‡]* *Yunosuke Nakahara,*[†] *Takahiro Sato,*[†] *Hironori Iwakura,*[†]
Shoya Takeshita,[‡] *Saki Minami,*[‡] *Hiroshi Yoshida,*[‡§] *Masato Machida*[‡§]*

[†] Catalysts Strategic Division, Engineered Materials Sector, Mitsui Mining & Smelting Co., Ltd.
[‡] Department of Applied Chemistry and Biochemistry, Graduate School of Science and Technology, Kumamoto University
[§] Unit of Elements Strategy Initiative for Catalysts & Batteries, Kyoto University
* E-mail: machida@kumamoto-u.ac.jp; y_nagao@mitsui-kinzoku.co.jp

Figure S1. XRD patterns of as-prepared a) $AlPO_4$, b) YPO_4, c) ZrP_2O_7 and d) $LaPO_4$.
Figure S2. *In situ* diffuse reflectance FT-IR spectra of adsorbed species formed on ZrP_2O_7 and ZrO_2 powders in gas mixtures of a) 0.8% C_3H_6, 0.5% O_2, and He balance (rich), b) 0.35% C_3H_6 + 3.25% O_2, and He balance (lean), and c) 1% C_3H_6 and He balance at 300 °C.
Figure S3. Fourier transforms of k^3-weighted Rh K-edge EXAFS of supported Rh catalysts without phase shift corrections.
Figure S4. FT-IR differential spectra of pyridine adsorbed onto ZrP_2O_7 and ZrO_2 at 50 °C and subsequent evacuation.
Table S1. Composition of simulated exhaust gas mixtures (NO-CO-C_3H_6-O_2-H_2-CO_2-H_2O) for 14.2 ≦ A/F ≦ 14.8 in test mode A.
Table S2. Composition of simulated exhaust gas mixtures (NO-CO-C_3H_6-O_2-CO_2-H_2O) for 14.6 ≦ A/F ≦ 15.3 in test mode B.
Table S3. Composition of simulated exhaust gas mixtures (NO-CO-O_2-CO_2-H_2O) for 14.6 ≦ A/F ≦ 15.3 in test mode C.
Table S4. Composition of simulated exhaust gas mixtures (NO-C_3H_6-O_2-CO_2-H_2O) for 14.6 ≦ A/F ≦ 15.3 in test mode D.
Table S5. Fitting results of Rh K-edge EXAFS analysis

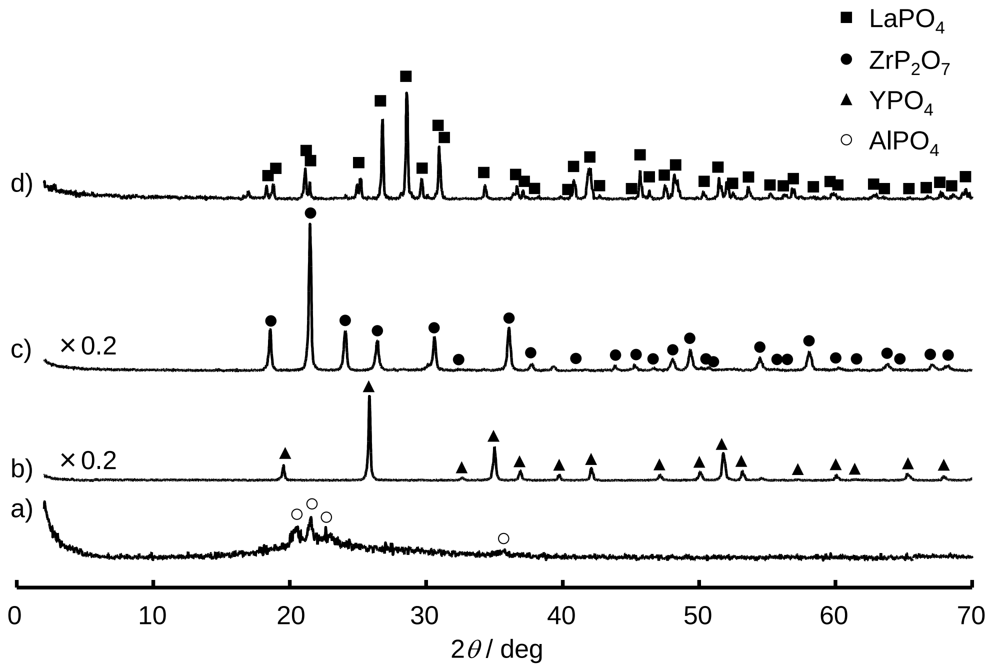

Figure S1. XRD patterns of as-prepared a) $AlPO_4$, b) YPO_4, c) ZrP_2O_7 and d) $LaPO_4$.

Figure S1 shows the XRD patterns of four types of metal phosphates after calcination. Diffraction peaks are attributed to monophasic metal phosphates with hexagonal $AlPO_4$ tridymite-type structure ($P6_3mc$, 5.097 Å, 8.344 Å)[1], tetragonal YPO_4 with xenotime-type structure, ($I4_1/amd$Z, 6.882 Å, 6.882 Å, 6.018 Å)[2], monoclinic $LaPO_4$ with monazite-type structure, ($P12_1/n$ 1, 6.825 Å, 7.057 Å, 6.482 Å, 103.2°)[3] and cubic ZrP_2O_7 (Pa-3, 8.293 Å)[4].

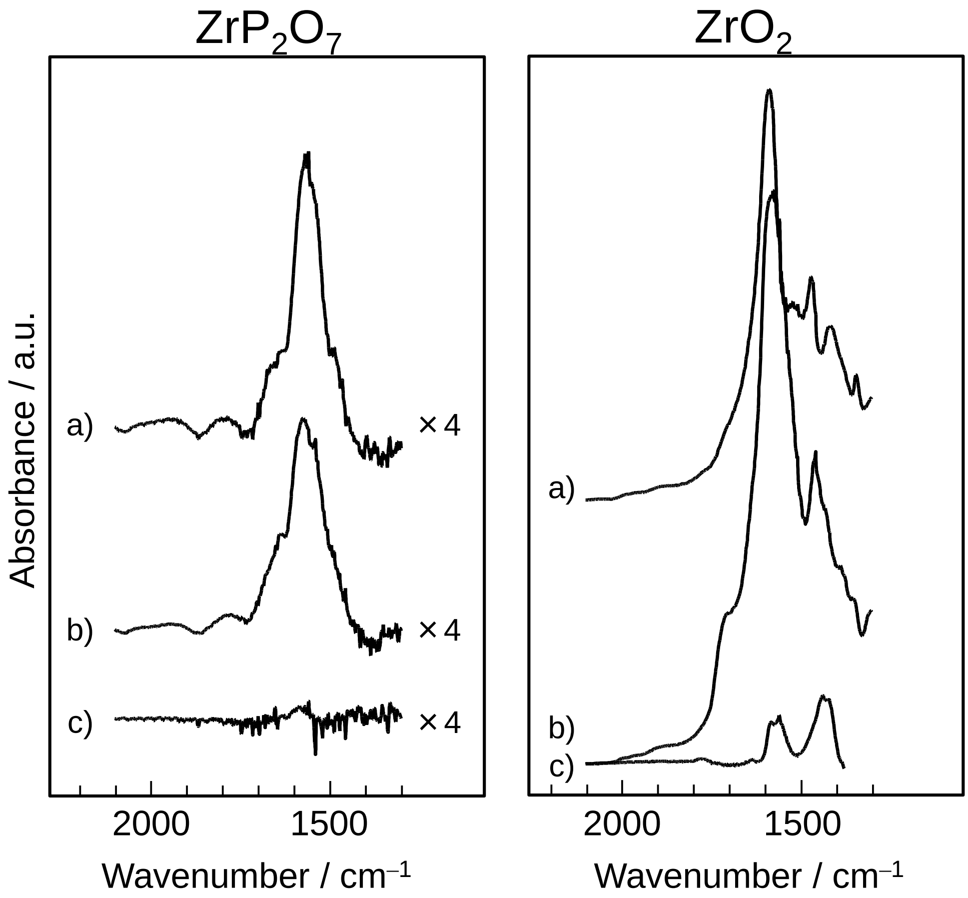

Figure S2. *In situ* diffuse reflectance FT-IR spectra of adsorbed species formed on ZrP_2O_7 and ZrO_2 powders in gas mixtures of a) 0.8% C_3H_6, 0.5% O_2, and He balance (rich), b) 0.35% C_3H_6 + 3.25% O_2, and He balance (lean), and c) 1% C_3H_6 and He balance at 300 °C.

C_3H_6 was adsorbed onto ZrP_2O_7 and ZrO_2 in the presence of O_2 to form aldehyde and carboxylate species, respectively. The intensity of observed bands for these Rh-unloaded support materials were as the same as those for Rh-loaded catalysts (**Figures 8 and 9**). These partially oxidized species were therefore adsorbed on the surface of support materials. Also, these species were formed in a similar way under the rich and lean conditions (a and b), but they were significantly decreased in the absence of O_2 (c).

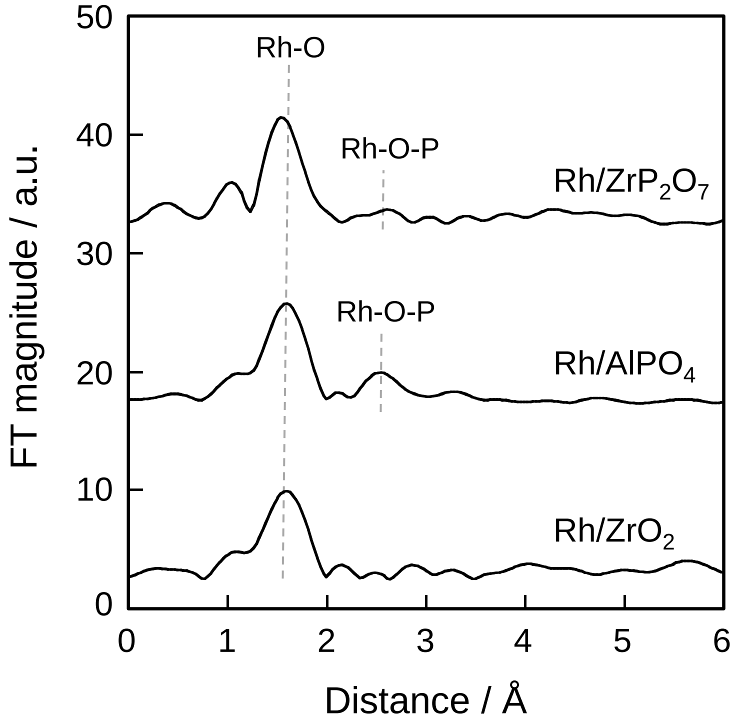

Figure S3. Fourier transforms of k^3-weighted Rh K-edge EXAFS of supported Rh catalysts without phase shift corrections. See **Table S5** for curve-fitting results and explanation of this figure.

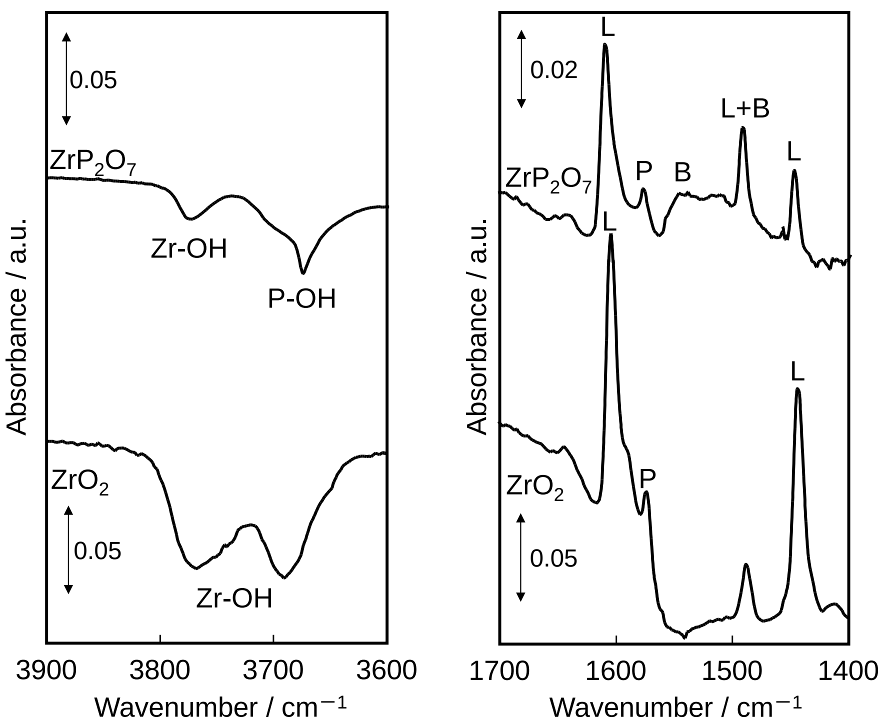

Figure S4. FT-IR differential spectra of pyridine adsorbed onto ZrP_2O_7 and ZrO_2 at 50 °C and subsequent evacuation. P: physisorbed pyridine, B: pyridine chemisorbed on Brønsted acid sites, L: pyridine chemisorbed on Lewis acid sites.

In situ FT-IR of pyridine chemisorption was carried out at 50 °C after dehydration at 500 °C in a He flow. The spectra obtained after subsequent evacuation at 50 °C were referenced to that of the sample in a He flow just before pyridine adsorption. ZrP_2O_7 yielded bands assignable to pyridine coordinated to Lewis acid site (L: 1610, 1492, and 1448 cm^{-1}) and to pyridinium ion adsorbed on Brønsted site (B: 1545, 1492 cm^{-1}) as reported by several researchers.[5-7] Simultaneously with the appearance of these bands, P−OH (3676 cm^{-1}) and Zr−OH (3773 cm^{-1}) bands were weakened. These results suggest that surface hydroxyl groups of ZrP_2O_7 act as both Lewis and Brønsted acid sites. By contrast, ZrO_2 yielded bands assigned only to Lewis acid site (L: 1604, 1488, and 1444 cm^{-1}).

Table S1. Composition of simulated exhaust gas mixtures (NO-CO-C_3H_6-O_2-H_2-CO_2-H_2O) for 14.2 ≦ A/F ≦ 14.8 in test mode A.

A/F [a]	14.2	14.4	14.5	14.6	14.7	14.8
CO / %	1.00	0.73	0.60	0.50	0.44	0.40
H_2 / %	0.33	0.24	0.20	0.17	0.15	0.13
C_3H_6 / ppm	400	←	←	←	←	←
NO / ppm	500	←	←	←	←	←
O_2 / %	0.35	0.41	0.45	0.50	0.55	0.60
CO_2 / %	14.0	←	←	←	←	←
H_2O / %	10.0	←	←	←	←	←

[a] The A/F value is calculated according to the literature[8] using following excess oxygen ratio of the simulated gas feed.

$$\text{Excess oxygen ratio} = \frac{\text{Amount of oxygen in gas feed}}{\text{Amount of oxygen required for complete oxidation}}$$

$$= \frac{2 \times p_{O2} + p_{NO}}{9 \times p_{C3H6} + p_{CO} + p_{H2}}$$

Table S2. Composition of simulated exhaust gas mixtures (NO-CO-C_3H_6-O_2-CO_2-H_2O) for 14.6 ≦ A/F ≦ 15.3 in test mode B.

A/F [a]	14.6	14.7	14.8	14.9	15.0	15.1	15.2	15.3
CO / %	0.69	0.59	0.52	0.52	0.50	0.40	0.40	0.30
C_3H_6 / ppm	400	←	←	←	←	←	←	←
NO / ppm	500	←	←	←	←	←	←	←
O_2 / %	0.50	0.55	0.60	0.69	0.81	0.84	0.96	0.93
CO_2 / %	14.0	←	←	←	←	←	←	←
H_2O / %	10.0	←	←	←	←	←	←	←

[a] See **Table S1**.

Table S3. Composition of simulated exhaust gas mixtures (NO-CO-O_2-CO_2-H_2O) for 14.6 ≦ A/F ≦ 15.3 in test mode C.

A/F [a]	14.6	14.7	14.8	14.9	15.0	15.1	15.2	15.3
CO / %	0.69	0.59	0.52	0.52	0.50	0.40	0.40	0.30
NO / ppm	500	←	←	←	←	←	←	←
O_2 / %	0.32	0.33	0.34	0.40	0.46	0.43	0.49	0.41
CO_2 / %	14.0	←	←	←	←	←	←	←
H_2O / %	10.0	←	←	←	←	←	←	←

[a] See **Table S1**.

Table S4. Composition of simulated exhaust gas mixtures (NO-C_3H_6-O_2-CO_2-H_2O) for 14.6 ≦ A/F ≦ 15.3 in test mode D.

A/F [a]	14.6	14.7	14.8	14.9	15.0	15.1	15.2	15.3
C_3H_6 / ppm	400	←	←	←	←	←	←	←
NO / ppm	500	←	←	←	←	←	←	←
O_2 / %	0.16	0.19	0.23	0.27	0.33	0.38	0.44	0.50
CO_2 / %	14.0	←	←	←	←	←	←	←
H_2O / %	10.0	←	←	←	←	←	←	←

[a] See **Table S1**.

Table S5. Fitting results of Rh K-edge EXAFS analysis

Catalyst	shell	CN [a] (±0.2)	r/Å [b] (±0.03)	$\sigma^2/10^{-2}$ Å^2 [c] (±0.02)
2 wt% Rh/ZrP_2O_7	Rh−O	2.9	2.01	0.15
	Rh−O−P	0.89	3.12	0.36
0.4 wt% Rh/$AlPO_4$	Rh−O	4.3	2.03	0.15
	Rh–Rh	0.32	2.69	0.42
	Rh–O–P	1.4	3.09	0.36
	Rh–O–Rh	0.19	3.54	0.64
2 wt% Rh/ZrO_2	Rh−O	4.1	2.04	0.15

Interval of k-space to r-space of FT is 3.0-14.0 Å^{-1}.
[a]Coordination number.
[b]Atomic distance.
[c]Debye-Waller factor.

Table S5 compares structural parameters for as-prepared supported Rh catalysts in **Figure S3**. These catalysts showed an intense peak at approximately 0.2 nm, which was attributed to a Rh–O shell of Rh oxide (Rh_2O_3). In the second coordination, a contribution of the Rh–O–P shell was observed in Rh/ZrP_2O_7 as was reported for Rh/$AlPO_4$ in our previous manuscript,[9] suggesting interfacial bonding between Rh and a phosphate unit (PO_4). Rh/ZrO_2 showed no such second coordination shell indicative of the metal-support bonding. The higher Rh loading (2 wt%) was used for Zr-containing supports to ensure the to ensure a good quality signal for curve fitting analysis.

References

1. Graetsch, H. A., *Acta Crystallogr. Sect. C: Cryst. Struct. Commun.* **2001,** *57*, 665-667.

2. Milligan, W. O.; Mullica, D. F.; Beall, G. W.; Boatner, L. A., *Inorg. Chim. Acta* **1982,** *60*, 39-43.

3. Mullica, D. F.; Milligan, W. O.; Grossie, D. A.; Beall, G. W.; Boatner, L. A., *Inorg. Chim. Acta* **1984,** *95*, 231-236.

4. Khosrovani, N.; Korthuis, V.; Sleight, A. W.; Vogt, T., *Inorg. Chem.* **1996,** *35*, 485-489.

5. Peri, J. B., *Discussions of the Faraday Society* **1971,** *52,* 55-65.

6. Bautista, F. M.; Campelo, J. M.; Garcia, A.; Luna, D.; Marinas, J. M.; Romero, A. A.; Navio, J. A.; Macias, M., *J. Catal.* **1994,** *145*, 107-125.

7. Campelo, J. M.; Garcia, A.; Herencia, J. F.; Luna, D.; Marinas, J. M.; Romero, A. A., *J. Catal.* **1995,** *151*, 307-314.

8. Tanaka, H.; Hirotoshi, F.; Takahashi, I., *SAE Paper* **1995**, 950256.

9. Machida, M.; Minami, S.; Ikeue, K.; Hinokuma, S.; Nagao, Y.; Sato, T.; Nakahara, Y., *Chem. Mater.* **2014,** *26*, 5799-5805.